Hindawi
Journal of Spectroscopy
Volume 2022, Article ID 1638042, 9 pages
https://doi.org/10.1155/2022/1638042

Research Article

Spectroscopic Study on the Species and Color Differences of Gem-Quality Red Garnets from Malawi

Ming Li

Jewelry Institute, Guangzhou Panyu Polytechnic, Guangzhou, China

Correspondence should be addressed to Ming Li; lm2020121002@126.com

Received 14 July 2022; Revised 22 August 2022; Accepted 19 September 2022; Published 27 September 2022

Academic Editor: K. S. V. Krishna Rao

To reveal the species of gem-grade red garnets with similar colors, especially the mechanisms underlying their subtle color differences, a series of tests, including conventional gemological tests, X-ray diffraction, Fourier-transform infrared spectroscopy, ultraviolet-visible spectroscopy, and X-ray photoelectron spectroscopy, were performed on gem-grade red garnets mined from Malawi. The results demonstrated that the color difference is not caused by the difference in species, and both the purplish-red and maroon-red garnets were magnesium-aluminum garnets (pyrope). They both contained the transition metal ions Fe^{2+}, Mn^{2+}, Fe^{3+}, and Cr^{3+}, with Fe^{2+} and Mn^{2+} occupying crystal site A and Fe^{3+} and Cr^{3+} occupying crystal site B. Cr^{3+} absorption peaks were observed at 367 and 690 nm; Fe^{3+} absorption peaks were observed at 502, 528, and 570 nm; and Mn^{2+} absorption peaks were observed at 400, 423, and 460 nm, which contributed to their respective colors. However, while the maroon-red pyrope had a larger Fe^{2+}/Fe^{3+} ratio than the purplish-red pyrope, it lacked Mn^{2+} ions, which is the cause of the color difference between the two pyrope garnets. To date, the study of color differences in red garnets remains a major controversial topic. This study proposed an innovative spectroscopic approach, particularly the combination of ultraviolet-visible spectroscopy and X-ray photoelectron spectroscopy, thus providing a novel methodology for investigating color differences in red garnets.

1. Introduction

The determination of garnet species is essential for the identification of jewelry and jade. The general chemical formula of garnets is $A_3B_2[SiO_4]_3$, where $A = Mg^{2+}$, Fe^{2+}, Mn^{2+}, Ca^{2+}, etc., and $B = Al^{3+}$, Cr^{3+}, Fe^{3+}, Ti^{3+}, V^{3+}, Zr^{3+}, etc., which leads to wide isomorphous substitution at these sites. Garnets are usually classified into six species in two series based on the combination of substitutions: (i) magnesium-aluminum garnet (pyrope), iron-aluminum garnet (almandine), and manganese-aluminum garnet (spessartine) in the aluminous series—Al^{3+} dominant at site B and (ii) calcium-aluminum garnet (grossular), calcium-iron garnet (andradite), and calcium-chromium garnet (uvarovite) in the calcareous series—Ca^{2+} dominant at site A [1–6]. Garnet species can usually be determined according to gemological parameters, such as color, refractive index, and relative density. For example, the normal base color of pyrope and almandine is red; however, they differ according to the shade of red. Some red garnets exhibit many other color shades, such as purplish-red and maroon-red. However, the refractive index, relative density, and other gemological parameters of these red garnets with uncommon color shades do not exactly meet the standard values specified for red garnets in the Chinese national standard, GB/T 16553 Gems–Testing. Therefore, it is difficult to identify them as specific mineral species in accordance with this standard, and they can only be called garnets in a general way or red garnets according to their color [7]. However, naming in this way is not advocated by the Chinese national standard; it is simply a stopgap for challenging samples. Therefore, determining the varieties of special garnets based on crystal chemistry principles expands our knowledge of garnets and is of scientific importance.

Previous research on garnet varieties and the causes of uncommon color shades have yielded controversial results [8–21]. For instance, gem-quality Chinese garnets mined from Muling, Heilongjiang Province, were identified as

(a) (b)

Figure 1: Malawi-mined (a) purplish-red and (b) maroon-red garnet samples.

pyrope garnets, and their maroon-red color was attributed to impurities: Cr^{3+}, Fe^{3+}, and Mn^{2+} ions [8]. Of the garnets mined in Mingxi, Fujian Province, the purplish-red varieties were also identified as pyrope garnets, and their purplish-red hue was attributed to a high Cr concentration [9]. Maroon-red varieties are a hybrid of pyrope and almandine garnets, and their coloration is due to high Fe and Ti contents [9]. Research on purplish-red and maroon-red garnets mined from Zambia indicated that they were both pyrope/almandine hybrids; it was found that the maroon-red varieties contained a higher content of Fe^{3+}, which resulted in stronger absorption at 425 nm in the violet region, which prevents the gemstone's transmission of violet light [10]. However, other studies have attributed absorption lines near 423 nm (at 425 nm) to Fe^{3+} and all absorption lines near 423 nm (at 430 nm) to Mn^{2+} [8–14]. Other studies on red garnet varieties have mainly relied on the content of key elements, such as Mg and Fe, to determine the varieties. Studies on the causes of color and color differences have linked colors and transition metal ions by comparing the absorption spectra of samples in the visible light region and the characteristic spectra of the transition metal ions possibly contained in the samples to infer which ions correspond to the absorption lines [18–21]. As such, the identification of absorption lines is key to investigating color differences in garnets. Therefore, in addition to understanding the characteristic absorption lines of transition metal ions, it is also necessary to determine the category, valence state, site occupancy, and chemical environment of the transition metal ions so that the absorption lines can be analyzed and accurately identified to reveal the impact of the transition metal ion chemical states on the color variations seen in red gem-quality garnets.

Although many purplish-red and maroon-red garnets mined from Malawi are referred to as pyrope garnets, their gemological parameters do not match those of standard pyropes according to conventional identification tests; they are usually intermediate between pyropes and almandines.

Therefore, this research aimed to investigate the gemological and spectroscopic characteristics of these purplish-red and maroon-red garnets to determine their varieties and the link between their color differences and the types, combination, and chemical states of the involved transition metal ions. This information provides a reliable theoretical basis that is useful for the identification of red series garnet varieties and to determine the causes of their color genesis and differences.

2. Materials and Methods

Malawi-mined natural, single-crystal garnets, including both raw crystals and faceted stones, purchased from a mining area in Malawi, were used for the experiments. The garnet samples were available in two common colors: purplish-red and maroon-red (Figure 1). Conventional gemological investigations of specific gravity, refractive index, extinction characteristic, and inclusions were performed on the garnet samples using the hydrostatic weighing method and a refractometer, polarizing microscope, and gem microscope. The X-ray powder diffraction (XRD) test was performed using the Bruker D8 ADVANCE XRD instrument at the Gemstone, Jade, and Jewelry Testing Center, Guangzhou Panyu Polytechnic. Garnet crystals were ground into powders with a particle size of ~10 μm in an agate mortar before the test. The test was performed using a Cu target, with a scanning voltage of 40 kV, a scanning current of 40 mA, a scanning speed of 2.5°/min, the 2θ range of 5°–70°, and a scanning step size of 0.05°. CuKβ was filtered out using the data processing software XrayRun2020. Infrared spectroscopy (IR) tests were performed using a Bruker Vertex 80 Fourier-transform infrared spectrometer, which comprised a solid substrate far-IR/Terahertz beam splitter, a broadband mid- and far-IR detector, and an UltraScanTM interferometer. The tests were performed in the KBr pellet transmission mode with a test region of 4000–400 cm^{-1}, a resolution of 4 cm^{-1}, and a number of scans of 32. The KBr

pellets were fabricated by pressing a 1 mg homogeneous mixture of garnet crystal powder and 150 mg potassium bromide powder on a pellet press. The ultraviolet-visible (UV-Vis) spectroscopy analysis was performed using a JASCO MSV5200 UV-Visible/NIR Microscopic spectrophotometer. Garnet crystals were ground into thin slices, ~0.5 cm thickness, and polished on both sides before the test. The tests were performed in the transmission mode with a test range of 300–1000 nm, a resolution of 1 nm, and a scanning speed of 600 nm/min. The IR and UV-Vis spectroscopies were both at the Hubei Jewelry Engineering Technology Research Center. The X-ray photoelectron spectroscopy (XPS) tests were performed using the ESCALAB 250Xi X-ray photoelectron spectrometer at the Materials Research and Testing Center, Wuhan University of Technology. Garnet crystals were wrapped in tin foil and then broken with pliers to obtain fresh sections before the test. Test conditions: AlKα ($E = 1253.6$ eV) was used as the X-ray radiation source, X-ray tube monitoring values were set at 14.2 kV and 11.3 mA, the instrument vacuum was below 10^{-7} Pa, the scanning step size was 0.05 eV, and the counting time was 1000 ms. Charge shift correction was made based on the electron binding energy (284.6 eV) of Cls. The energy range of the full-spectrum scan was 0–1200 eV. Considering that the analyzed objects were mainly trace elements, the photoelectron energy spectral lines of these trace elements were finely scanned and superimposed 32 times to improve their resolution. The XPS element analysis range was Li–U, and the detection limit is generally 0.1% (atomic percent).

3. Results

3.1. Gemological Characteristics. Both types of garnet samples exhibited vibrant and uniformly scattered purplish-red and maroon-red shades. The crystals were spherical, with various grain sizes, usually around 1 cm. The bulk had been rounded by external pressure; however, the crystal faces of some were preserved, being a monomorphic occurrence as tetragonal trisoctahedrons. The relative density tests indicated that the relative densities of the purplish-red and maroon-red crystals were 3.87 and 3.83, respectively. Both types of crystals exhibited a glass-like sheen and a high degree of transparency. Observations under the gem microscope showed that while both types of crystals contained a few gas-liquid inclusions, the purplish-red crystals contained more short needle-like inclusions. Both crystals show a complete extinction phenomenon under a polarizing microscope. The refractive indices of the purplish-red and maroon-red crystals were 1.762 and 1.757, respectively, both of which were slightly different from the common pyrope (1.714–1.742) [17].

3.2. X-Ray Diffraction Analysis. The X-ray powder diffraction patterns of the purplish-red and maroon-red garnets, along with the d-values of the main diffraction peaks and the corresponding crystallographic planes, were consistent with the X-ray powder diffraction patterns PDF73-2367 and PDF73-2368, respectively, which both indicated pyrope garnets (see Figure 2). In addition, the sharp, symmetrical diffraction peaks suggested that both the purplish-red and maroon-red pyrope were well crystallized.

3.3. Fourier-Transform Infrared Spectroscopy Analysis. Fourier-transform infrared (FT-IR) spectroscopy was performed on the garnet samples in fingerprint regions and the spectrum is shown in Figure 3. Assigned absorption bands interpreted according to previous research studies [22–27] are shown in Table 1.

The garnet samples had three strong, independent absorption peaks in the range of 850–1000 cm^{-1} and medium-strong absorption peaks in the higher wavenumber range of 610–650 cm^{-1}. These absorption peaks were at ~ 970, ~904, ~874, ~644, ~571, ~532, ~477, and ~456 cm^{-1}. The absorption peaks for garnet samples were similar to the IR spectra of pyrope despite minor peak shifts in some peaks. However, the IR spectrum of the garnet samples was not in complete agreement with the standard IR spectra of pyrope [24], with four additional peaks at 532, 534, 608, and 644 cm^{-1} absent in that of pyrope.

The IR spectrum showed differences between purplish-red and maroon-red garnets. The purplish-red garnet had an extra peak at 608 cm^{-1}, and the peak positions of the maroon-red garnet at 456, 532, 571, and 967 cm^{-1} were lower than the corresponding peaks of the purplish-red garnet by about four-wave numbers.

3.4. Ultraviolet-Visible Spectroscopy Analysis. The garnet samples were analyzed to obtain their ultraviolet-visible (UV-Vis) absorption spectrum (Figure 4). The garnet samples were cut into parallel slabs at 5 mm in thickness and treated without orientation because they were optically isotropic materials. Both types of garnet samples exhibited a broad absorption band with a relatively good symmetry at 690 nm in the red region; at 570, 528, and 502 nm in the yellow-green region; and at 367 nm in the violet region, with strong transmission near 655 nm in the red region. Both garnets had a reddish color due to this selective light absorption.

However, in addition to the above absorption and transmission, unlike the maroon-red garnet, the purplish-red garnet also exhibited narrower but distinct absorptions at 460, 423, and 400 nm in the blue-violet region, particularly in the violet region, with comparatively strong transmissions near 445 and 385 nm. The purple color of the purplish-red garnet was caused by such a variation in selective absorption. We also noticed that the absorption peaks of the maroon-red garnet at 570, 528, and 502 nm in the yellow-green region were significantly weaker than those of the purplish-red garnet, which may be attributable to the difference in the contents of the relevant ions.

3.5. X-Ray Photoelectron Spectroscopy Analysis. X-ray photoelectron spectroscopy (XPS) was conducted on fresh sections of the garnet samples. A broad-spectra scan was initially performed to detect the chemical elements in the samples, followed by an intensively narrowed spectrum scan to determine the chemical states of the transition metal

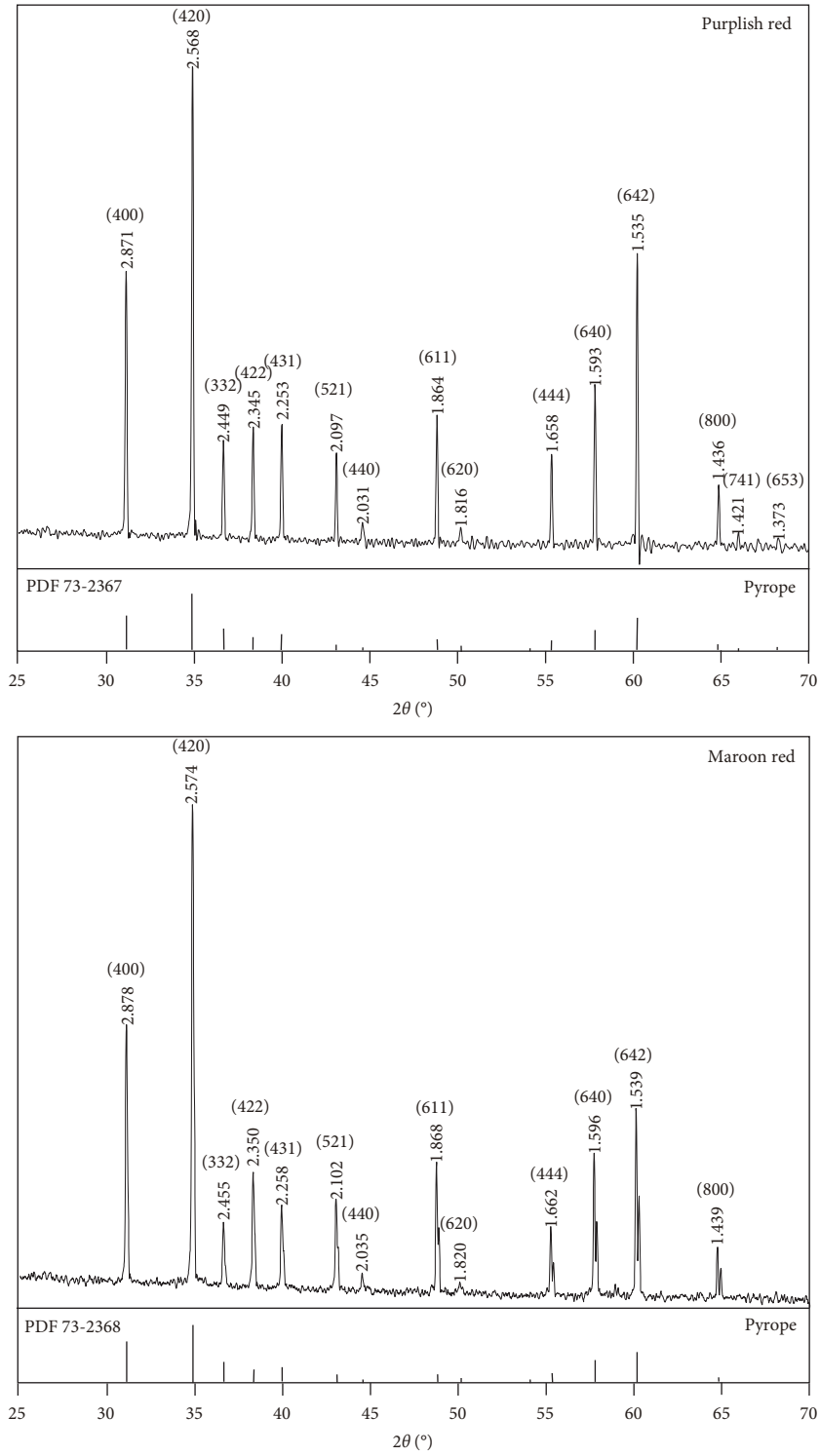

Figure 2: X-Ray powder diffraction spectra of the garnet samples.

elements in the samples. Figure 5 depicts the wide XPS spectrum of the samples. The results revealed that both the purplish-red and maroon-red garnets mainly contained Mg, Fe, Al, Si, and O. However, the purplish-red garnet had a stronger Mg signal and a weaker Fe signal compared to the maroon-red garnet.

The typical XPS spectra of the transitional metal cations are shown in Figure 6. An in-depth scan confirmed that the purplish-red garnet sample also contained a small amount of the element Mn, while the maroon-red sample did not. Furthermore, while both garnets contained the element Fe, the chemical states of the Fe differed.

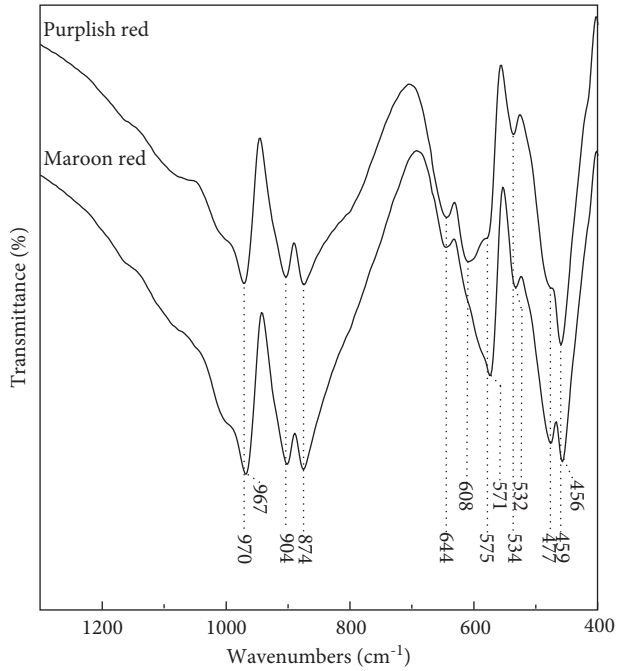

Figure 3: Fourier-transform infrared spectrum of the garnet samples.

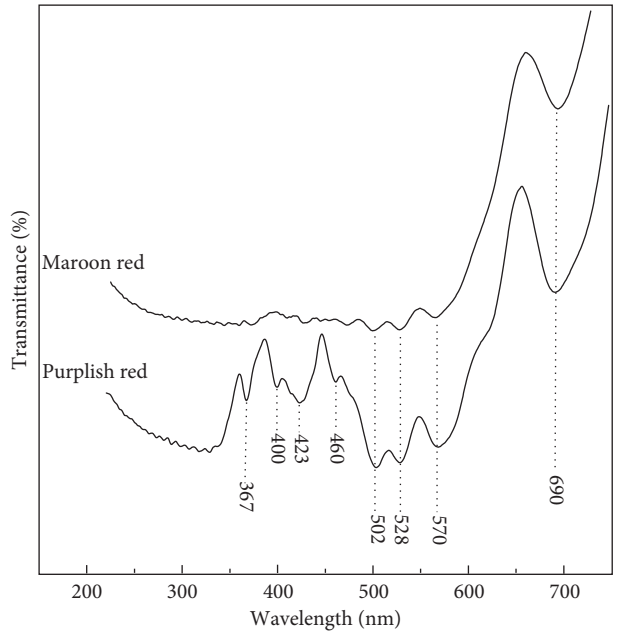

Figure 4: Ultraviolet-visible spectra of the purplish-red and maroon-red garnets.

Table 1: Characteristics and attributes of the infrared absorption peaks of the purplish-red and maroon-red garnets.

Absorption peaks of the garnet samples (cm^{-1})		Attributions of the absorption peaks	Absorption peaks of the pyrope end-member [24]
Purplish-red	Maroon-red		
970	967		964
904	904	ν_{as} (Si–O–Si)	893
874	874		865
644	644		—
608	—		—
575	571	δ_{as} (Si–O–Si)	570
534	532		—
477	477		477
459	456	δ (Al–O–Si)	452

The XPS peak of Fe2p3/2 was asymmetric, and the peak asymmetry of the purplish-red garnet differed from that of the maroon-red garnet (Figure 6(a)). The strong shoulder peak on the high binding energy side of the maroon-red garnet spectra and the low binding energy side of the purplish-red garnet implied that the Fe2p3/2 peaks in the spectra were composite peaks. The results of peak-differentiation-imitation [28] showed that the composite peaks can be fitted by two peaks at 709.9 and 711.3 eV, corresponding to the electron binding energies of Fe2p3/2, 709.6, and 711.4 eV, in the structures of the FeO [29] and Fe_2O_3 [30] compounds, respectively. This indicated that the Fe elements in both the purplish-red and maroon-red garnet samples had two valency states, Fe^{2+} and Fe^{3+}, both of which were coordinated with O ions to form bonds. However, the Fe^{2+}/Fe^{3+} ratios of the two garnets differed. The Fe in the maroon-red garnet was predominantly Fe^{2+}, while the proportion of Fe^{3+} was higher in the purplish-red garnet. According to the results of the peak-differentiation-imitation, the Fe^{2+}/Fe^{3+} ratios were 1.11 and 0.54 in the maroon-red and purplish-red garnet samples, respectively.

The XPS spectra for Mn2p are shown in Figure 6(b). Weak signals of the element Mn were only identified in the purplish-red garnet sample, suggesting that, in addition to the Fe element, the purplish-red garnet also contained a small amount of Mn. In contrast to the Fe2p3/2 peak, the peak shape of Mn2p presented a high degree of symmetry, and the peak position of Mn2p3/2 was 641.7 eV, which corresponded to the electron binding energy of Mn2p3/2 in MnO [31]. This revealed that the Mn elements in the purplish-red sample existed as Mn^{2+} and were mostly coordinated with O ions to form bonds.

The XPS spectrum of Cr2p is shown in Figure 6(c). Weak signals of elemental Cr were discovered in both the purplish-red and maroon-red garnet samples, indicating that both garnets contained trace amounts of Cr. In contrast to the Fe2p3/2 peak,

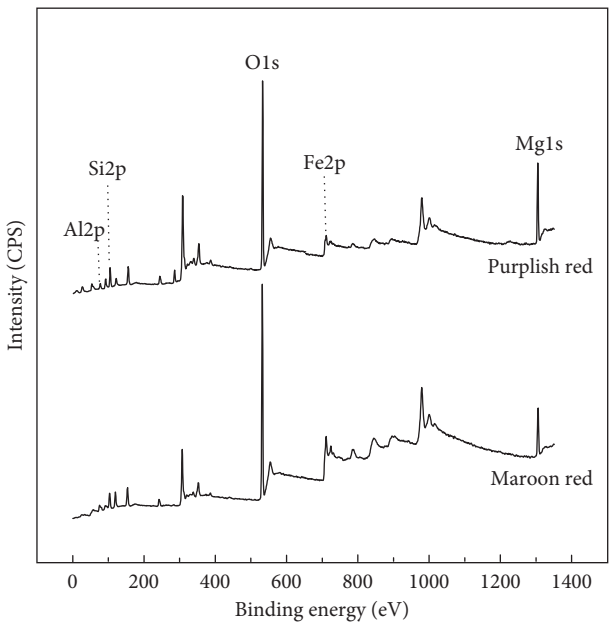

Figure 5: X-ray photoelectron spectrum of the garnet samples.

there was no evident asymmetry in the shape of the Cr2p peak and the electron binding energy of Mn2p3/2.

In the typical compound, $CrBO_3$ is 577.9 eV for the Cr2p3/2 peak locations. This indicates that the Cr elements in both the purplish-red and maroon-red garnet samples existed as Cr^{3+} and were mostly coupled to O ions to form bonds [32].

4. Discussion

4.1. Identification of Red Garnet Varieties. Although it would be difficult to identify the varieties of the garnets examined in this study using conventional gemstone identification methods, identifying the varieties of these special garnets is of scientific significance. According to the analysis of gemological properties, the relative densities of the red garnet samples (purplish-red garnet: 3.87; maroon-red garnet: 3.83) were within the reference range for pyrope (3.62–3.87) provided by the Chinese national standard, GB/T 16553 Gems–Testing. However, both refractive indices (purplish-red garnet: 1.762; maroon-red garnet: 1.757) were outside the GB/T 16553 standard reference range for pyrope (1.714–1.742) and the refractive index of the purplish-red sample entered the reference range for almandine (1.760–1.820) [17]. In this case, it is difficult to identify them as specific mineral varieties in accordance with this standard and they can only be called garnets in a general way or red garnets according to their color [7].

However, the XRD and FT-IR spectra clearly showed that both the purplish-red and maroon-red garnets mined from Malawi were pyrope garnets. Moreover, the results of the FT-IR analysis matched well with the refractive indices of the samples, which exceeded the GB/T 16553 reference range for pyrope. The infrared spectra of the two samples contained four additional absorption peaks at 532, 534, 608, and 644 cm^{-1} compared to the standard pyrope spectrum. These four additional absorption peaks were very similar to those of the standard FT-IR spectra of almandine and spessartine, which indicated that these pyrope garnets were not end-member pyropes and that they contained extensive isomorphous substitution by Fe and Mn. The substitution of Mg by Fe and Mn can increase the refractive index of garnet [1].

As described in the introduction, previous studies on similar red garnet varieties have also shown that such garnets were pyrope or a hybrid of pyrope and almandine garnets [8–14]. In summary, the results of this study suggest that both the purplish-red and maroon-red garnets mined from Malawi were pyrope garnets with extensive isomorphous substitution by Fe and Mn.

4.2. Causes of Color Variation in Red Garnets. The causes of the color difference between the purplish-red and maroon-red garnets in terms of absorption spectrum were determined by the results of the UV-Vis spectroscopy. Both types of garnets produced a broad absorption band with good symmetry at 690 nm in the red region; at 570, 528, and 502 nm in the yellow-green region; and at 367 nm in the purple region, with strong transmission near 655 nm in the red region. This is why both garnets have a reddish color. However, in addition to these absorptions and transmissions, unlike the maroon-red garnets, the purplish-red garnets also formed narrower but distinct absorptions at 460, 423, and 400 nm in the blue-violet region, particularly in the violet region, with comparatively strong transmissions near 445 and 385 nm. The purple of the purplish-red garnet was caused by such variation in selective absorption. The color of a mineral is the result of its selective absorption of visible light, which is often caused by the transitional metal elements contained in the mineral [33].

In previous studies [8–10] on the color genesis and causes of color differences in red garnets, the absorption spectra of red garnets mined from Muling, Heilongjiang, China; Mingxi, Fujian, China; and Zambia were not significantly different from those obtained in the current study, with only small differences in the presence and position of a few absorption peaks.

However, obvious differences were found in the attribution of the absorption lines. For example, the additional three absorption lines seen in the spectrum of the purplish-red sample at 460, 423, and 400 nm compared to the maroon-red sample have been attributed to absorption lines near 400 nm (at 407 nm), near 423 nm (at 425 nm), and near 460 nm (at 461 nm) to Mn^{2+}, Fe^{3+}, and Fe^{2+}, respectively [14, 15]. However, it was also suggested that both absorption lines, one near 423 nm (at 430 nm) and one at 460 nm, were attributable to Mn^{2+} [8, 11, 12].

In comparison, the purplish-red garnet had three more absorption lines, at 460, 423, and 400 nm, compared to the maroon-red garnet. Unlike the maroon-red garnet, the purplish-red garnet contained Mn^{2+} ions occupying crystal site A, and the three additional absorption lines matched well with the characteristic spectral lines of Mn^{2+} ions. Thus, we inferred that the three absorption lines at 460, 423, and

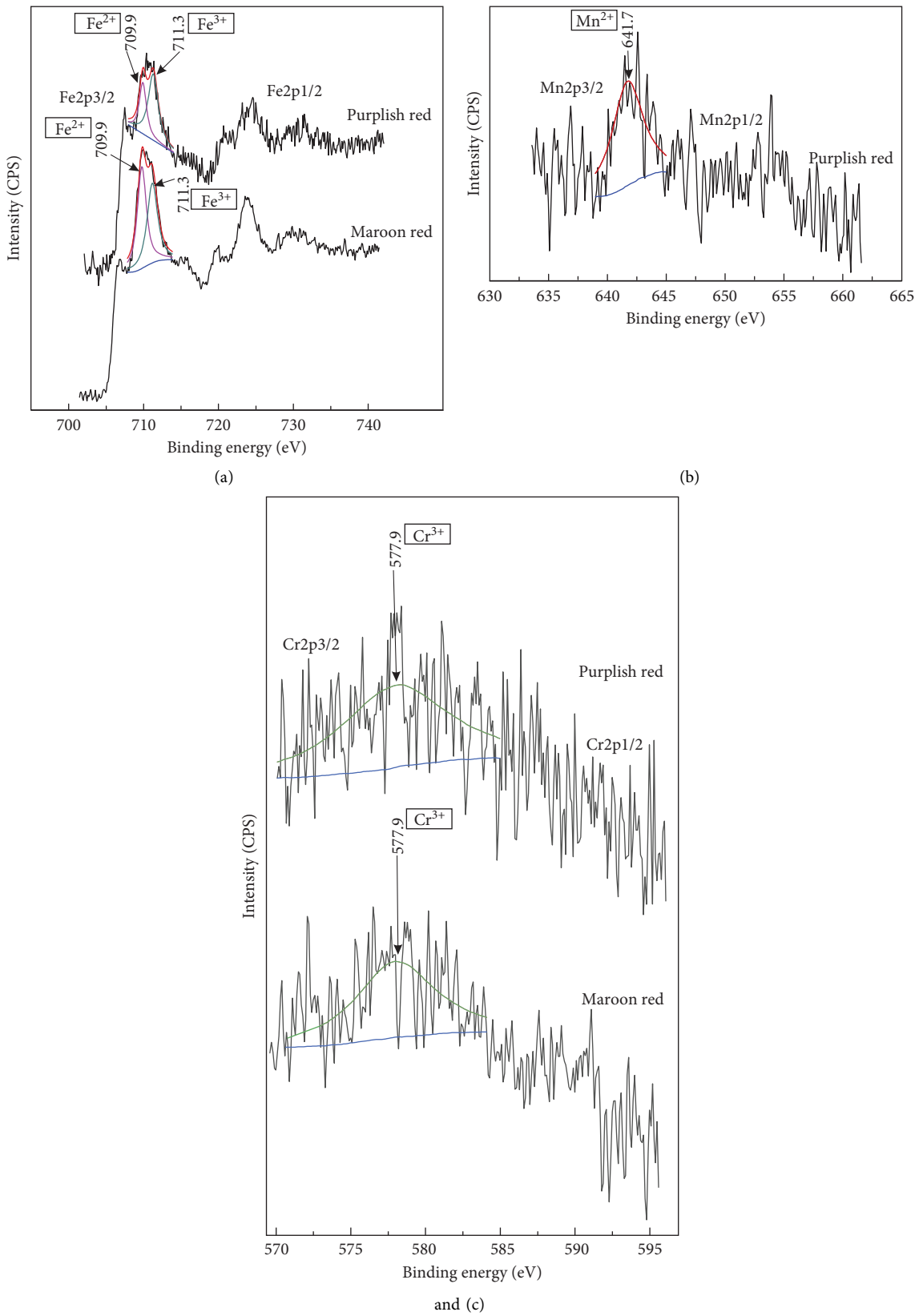

Figure 6: X-ray photoelectron spectra for Fe2p, Mn2p, and Cr2p. ((a) Fe2p, (b) Mn2p, and (c) Cr2p).

400 nm were caused by the d-d electron transition of Mn^{2+} [8, 11]. Therefore, the Mn^{2+} ions must have contributed to the color difference between the purplish-red and maroon-red garnets. However, it should be noted that (i) the isomorphous substitution by Mn^{2+} ions identified in the purplish-red garnet was not identified in the maroon-red garnet; (ii) according to the FT-IR spectrum, the purplish-red garnet had an additional absorption peak at 608 cm^{-1} compared to the maroon-red garnet; and (iii) the purplish-red garnet had a higher refractive index than the maroon-red garnet (1.762 > 1.757).

These differences support each other well. In terms of IR spectra, although the Si–O bonding force inside SiO_4 tetrahedra is significantly greater than the bonding force between ions at sites A and B and SiO_4 tetrahedra, the ions at sites A and B and the generated polyhedra surrounding them have various degrees of influence on the SiO_4 tetrahedral vibrations [25, 26]. The purplish-red garnet had additional Mn^{2+} ions at crystal site A, which were not found in the maroon-red garnet, resulting in a more complex δ_{as} (Si–O–Si) structure. In terms of refractive index, the Mn^{2+} ions at crystal site A were able to increase the refractive index of the purplish-red garnet [1].

XPS analysis also showed that both the purplish-red and maroon-red garnets contained Fe^{2+}, Fe^{3+}, and Cr^{3+}. Garnets are nesosilicate minerals with an isometric crystal structure. In the crystal structure, the island-like distributed SiO_4 tetrahedra are linked together by octahedra centered on trivalent cations (ions at site B) and dodecahedra (distorted cubes) centered on divalent cations (ions at site A). In the crystal structure of both the purplish-red and maroon-red garnets, Fe^{2+} and Mn^{2+} inhabited site A, whereas Fe^{3+} and Cr^{3+} occupied site B. These ions were mostly coordinated to form connections with O ions. That is to say, the Fe^{2+}, Fe^{3+}, and Cr^{3+} in the purplish-red and maroon-red garnets had the same chemical state, which was why the two garnets shared some similar parts of their absorption spectra [11, 12, 34–37]. According to previous research, the absorption peaks at 367 and 690 nm were created by Cr^{3+}, which has a $3d^3$ electronic structure. The distinctive Cr^{3+} spectrum is produced by the energy-level transition of the spectral component $^4A_{2g}$ (4F). Among these transitions, the $^4A_{2g}$ (4F) $\longrightarrow$ $^4T_{2g}$ (4F) transition produces an absorption peak at 690 nm, and the $^4A_{2g}$ (4F) $\longrightarrow$ $^4T_{1g}$ (4P) transition produces an absorption peak at 367 nm [11]. In addition, the absorption peaks at 502, 528, and 570 nm were caused by the forbidden d–d electron transition of Fe^{3+}. Fe^{2+} has a $3d^6$ configuration and usually appears colorless in cubic symmetric compounds, whereas Fe^{3+} has a $3d^5$ configuration, and its compounds usually appear brown [12].

The maroon-red garnet had a relatively higher Fe^{2+}/Fe^{3+} ratio than the purplish-red garnet, which matched well with the peak positions of the maroon-red garnet at 456, 532, 571, and 967 cm^{-1}, which were lower than the corresponding peaks of the purplish-red garnets by around three wave numbers, and the UV-Vis analysis absorption peaks of the maroon-red garnet at 570, 528, and 502 nm in the yellow-green region were weaker than those of the purplish-red garnet. In terms of FT-IR spectra, previous research has shown that the wave numbers of SiO_4 tetrahedral vibrations within the range of 1500–400 cm^{-1} increase in the sequence of andradite, grossular, spessartine, almandine, and pyrope. An increase in Fe^{2+} content could have decreased the positions of the relevant infrared absorption peaks in the maroon-red garnet [38, 39], and a decrease in the Fe^{3+} content could have diminished the intensity of the UV-Vis spectra absorption peaks.

5. Conclusions

(1) Both the purplish-red and maroon-red garnet samples mined from Malawi are pyrope garnets and contain the transition metal ions Fe^{2+}, Mn^{2+}, Fe^{3+}, and Cr^{3+}, with Fe^{2+} and Mn^{2+} occupying site A and Fe^{3+} and Cr^{3+} occupying site B in the crystal structure.

(2) The absorption peaks created by Cr^{3+} at 367 and 690 nm; by Fe^{3+} at 502, 528, and 570 nm; and by Mn^{2+} at 400, 423, and 460 nm in both pyrope garnets contributed to their respective colors.

(3) The color difference was caused by the maroon-red pyrope garnet having a higher Fe^{2+}/Fe^{3+} ratio compared to the purplish-red pyrope and the lack of Mn^{2+} ions and their corresponding absorption peaks in the maroon-red pyrope garnet.

Data Availability

The data set is presented directly in the present study.

Conflicts of Interest

The authors declare that there are no conflicts of interest with any institution or funding body.

Acknowledgments

This work was supported by the Natural Science Foundation of Guangzhou Panyu Polytechnic (Grant no. 2021KJ09).

References

[1] B. L. Zhang, *Systematic Gemmology*, Geology Press, Beijing, China, 2rd edition, 2006.

[2] E. S. Grew, A. J. Locock, S. J. Mills, I. O. Galuskina, E. V. Galuskin, and U. Haleniu, "Nomenclature of the garnet supergroup," *American Mineralogist*, vol. 98, pp. 785–811, 2013.

[3] A. G. Shtukenberg, Y. O. Punin, O. V. Frank-Kamenetskaya, O. G. Kovalev, and P. B. Sokolov, "On the origin of anomalous birefringence in grandite garnets," *Mineralogical Magazine*, vol. 65, no. 3, pp. 445–459, 2001.

[4] R. Brightman, "A new variety of grossular garnet with extended gemological constants," *The Australian Gemmologist*, vol. 19, pp. 19–22, 1995.

[5] C. R. Bridges, "Green grissularite garnets (tsavorites) in East Africa," *Gems and Gemology*, vol. 14, pp. 290–296, 1974.

[6] B. W. Anderson, "Transparent green grossular-a new gem variety; together with observations on translucent grossular

and idocrase," *Journal of Gemmology*, vol. 10, no. 4, pp. 113–119, 1966.

[7] N. Jewelry and Jade Standardization Technical Committee, *Gems-Testing: GB/T 16553-2017*, China Quality and Standards Publishing and Media Co., Ltd, Beijing, China, 2017.

[8] T. Chen, Y. G. Liu, Z. W. Yin, and N. Liu, "Gemology and spectra characterization of gem garnet from muling City, Heilongjiang Province," *Spectroscopy and Spectral Analysis*, vol. 33, no. 11, pp. 2964–2967, 2013.

[9] D. P. Tang, A. G. Jiang, and W. Y. Luo, "The gemological features of the garnets from Mingxi, Fujian," *J. F. Oberlin University*, vol. 29, pp. 64–66, 2001.

[10] Y. Zhong, M. W. Qu, and X. T. Shen, "Comparison of chemical composition and spectroscopy of purple-brownish red garnet from Zambia, Tanzania and Australia," *Spectroscopy and Spectral Analysis*, vol. 42, pp. 184–190, 2022.

[11] C. A. Geiger, A. Stahl, and G. R. Rossman, "Single-crystal IR- and UV/vis-spectroscopic measurements on transition-metal-bearing pyrope: the incorporation of hydroxide in garnet," *European Journal of Mineralogy*, vol. 12, no. 2, pp. 259–271, 2000.

[12] X. M. He and L. S. Lv, "Mineralogical characteristics and the coloring mechanism of uvarovite from eastern Tibet, China," *Earth Science Frontiers*, vol. 14, pp. 246–253, 2007.

[13] M. W. Qu, Y. Zhong, and X. T. Shen, "Gemmological characteristic of purple-brownish red garnet from Zambia," *Journal of Gems & Gemmology*, vol. 23, pp. 20–28, 2021.

[14] R. K. Moore and W. B. White, "Electronic spectra of transition metal ions in silicate garnets," *The Canadian Mineralogist*, vol. 11, pp. 791–811, 1972.

[15] J. W. Yin, H. K. Lee, K. K. Chio, and S. J. Kim, "Characteristics of garnet in shizhuyuan skarn deposit, hunan Province," *Journal of Environmental Sciences*, vol. 25, pp. 163–171, 2000.

[16] L. Zhu, *The Study on Gemological Characteristic of Red to Yellow Series Garnets. Master*, China University of Geosciences, Beijing, China, 2015.

[17] Y. M. Chen, X. Y. Yu, Y. Yang, and C. T. Ruan, "A study of gemological and mineralogical characteristics and color zonation of garnets from Jinan, Shandong Province," *Acta Petrologica et Mineralogica*, vol. 40, pp. 581–592, 2021.

[18] G. C. Chi, Y. Wu, and J. F. Hu, "The characteristics and classification of garnets from kimberlite in Mengyin, Shandong Province," *Acta Petrologica et Mineralogica*, vol. 33, pp. 877–884, 2014.

[19] G. C. Chi, G. W. Li, G. Xiao et al., "The characteristics and varieties identification of garnets hosted in the kimberlites from Wafangdian," *Liaoning Province. Rock and Mineral Analysis*, vol. 32, pp. 78–83, 2013.

[20] I. Adamo, A. Pavese, L. Prosperi, V. Diella, and D. Ajó, "Gem-quality garnets: correlations between gemmological properties, chemical composition and infrared spectroscopy," *Journal of Gemmology*, vol. 30, no. 5, pp. 307–319, 2007.

[21] M. L. Johnson, E. Boehm, H. Krupp, J. W. Zang, and R. C. Kammerling, "Gem-quality grossular-andradite: a new garnet from Mali," *Gems and Gemology*, vol. 31, no. 3, pp. 152–166, 1995.

[22] X. X. Yan, S. W. Yue, and S. Y. Chen, "Spectroscopic characteristics and coloring mechanism of color-change garnet," *Laser and Optoelectronics Progress*, vol. 59, Article ID 133301, 2022.

[23] J. R. Wang, Y. M. Wang, D. Q. Zhang et al., "FTIR investigation of garnet: indication for specific varieties and coloration: a case study of a yellow garnet," *Journal of Gems & Gemmology*, vol. 22, pp. 20–25, 2020.

[24] W. S. Peng and G. K. Liu, *Mineral Infrared Spectral Atlas*, Science Press, Beijing, China, 1982.

[25] A. M. Hofmeister and A. Chopelas, "Vibrational spectroscopy of end-member silicate garnets," *Physics and Chemistry of Minerals*, vol. 17, no. 6, pp. 503–526, 1991.

[26] S. J. Gao, L. N. Zhai, and L. Ying, "Infrared spectrum of garnet from the Xihuashan granite," *Minerals and Rocks*, vol. 7, pp. 112–116, 1987.

[27] B. P. McAlooN and A. M. Florurrsrn, "Single-crystal IR spectroscopy of grossular-andradite garnet," *American Mineralogist*, vol. 80, pp. 1145–1156, 1995.

[28] M. C. Biesinger, B. P. Payne, A. P. Grosvenor, L. W. M. Lau, A. R. Gerson, and R. S. C. Smart, "Resolving surface chemical states in XPS analysis of first row transition metals, oxides and hydroxides: Cr, Mn, Fe, Co and Ni," *Applied Surface Science*, vol. 257, no. 7, pp. 2717–2730, 2011.

[29] P. Mills and J. L. Sullivan, "A study of the core level electrons in iron and its three oxides by means of X-ray photoelectron spectroscopy," *Journal of Physics D: Applied Physics*, vol. 16, no. 5, pp. 723–732, 1983.

[30] G. C. Allen, M. T. Curtis, A. J. Hooper, and P. M. Tucker, "X-Ray photoelectron spectroscopy of iron–oxygen systems," *Journal of the Chemical Society Dalton Transactions*, vol. 14, pp. 1525–1530, 1974.

[31] B. J. Tan, K. J. Klabunde, and P. M. A. Sherwood, "XPS studies of solvated metal atom dispersed (SMAD) catalysts. Evidence for layered cobalt-manganese particles on alumina and silica," *Journal of the American Chemical Society*, vol. 113, no. 3, pp. 855–861, 1991.

[32] T. P. Moffat, R. M. Latanision, and R. R. Ruf, "An X-ray photoelectron spectroscopy study of chromium-metalloid alloys—III," *Electrochimica Acta*, vol. 40, no. 11, pp. 1723–1734, 1995.

[33] K. Nassau, "The origins of color in minerals," *American Mineralogist*, vol. 63, pp. 219–229, 1978.

[34] D. R. Kanungo, D. B. Malpe, and C. J. Radhakrishnan, "Chrome-rich green garnets from mesoproterozoic sausar fold belt, tirodi area, Central India," *Journal of the Geological Society of India*, vol. 69, pp. 65–69, 2007.

[35] V. W. Lueth and R. Jones, "Red grossular from the sierra de Cruces, coahuila, Mexico," *The Mineralogical Record*, vol. 34, pp. 73–95, 2003.

[36] H. Q. Wu, *The Study on Gemological Characteristic and Color Genesis of Orange to Red Series of Garnets. Master*, China University of Geosciences, Beijing, China, 2016.

[37] P. G. Manning, "Optical absorption spectra of Fe^{3+} in octahedral and tetrahedral sites in natural garnets," *The Canadian Mineralogist*, vol. 11, pp. 826–839, 1972.

[38] X. X. Yan, P. L. Wang, and S. W. Yue, "Spectroscopic characteristics and coloring mechanism of Greenish–Yellow beryl under heating treatment," *Spectroscopy and Spectral Analysis*, vol. 40, pp. 3795–3800, 2020.

[39] L. G. Qu, L. Xu, J. G. Liu et al., "Numerical simulation analysis of portable high-speed FTIR rotary interfero-meters," *Acta Optica Sinica*, vol. 41, Article ID 0907001, 2021.